Synthetic modification of fusogenic coiled coil peptides

Crone, N.S.A.

Photoswitchable β-sheet forming peptides

This chapter is in preparation as an original research paper: Niek S.A. Crone, Mousumi Samanta, Dinghao Wu, Elena Egorova, Panagiota Papadopoulou, Aimee L. Boyle, Gonen Ashkenasy, Alexander Kros, **2022**.

Abstract

Controlling the folding of β-sheet peptides is of interest as a tool for the generation of responsive (bio)materials. The change in structure and polarity associated with azobenzene photoisomerization was hypothesized to disrupt β-sheet self-assembly when substituting other hydrophobic amino acids. To test this hypothesis, peptides were prepared based on the $(EF)_5EP$ peptide sequence which is known to form β-sheet fibres. Modification of a single phenylalanine to an azobenzene resulted in peptide self-assembly at lower salt concentrations. Both β-structure and critical aggregation concentration could be altered via photoisomerization, with the biggest effect observed with the azobenzene positioned in the peptide centre. Azobenzene-containing peptides showed self-assembly as peptide fibres, with fibre oligomerization observed when the azobenzene was positioned at the peptide terminus. Histidine containing peptide variants were subsequently prepared, and showed organocatalytic activity in ester hydrolysis that could be altered by azobenzene isomerization. Together, this study demonstrates the incorporation of amino acids carrying azobenzene moieties as a novel method for active control over β-structure, peptide self-assembly and activity.

6.1 Introduction

Peptides and proteins adopt three-dimensional structures in order to minimize backbone steric clashes, maximize potential hydrogen bonding interactions and facilitate favourable side-chain interactions.[1] One of the most dominant folds is the β-sheet, consisting of multiple β-strands connected laterally through hydrogen bonds between backbone peptide amides. Each amino acid can be defined by its tendency to fold into α-helices or β-structures,[2] but the pattern in which polar and hydrophobic amino acids are repeated is what predominantly determines the type of fold.[3] In the previous chapters the focus has been on controlling the folding and oligomerization of α-helical coiled-coil peptides, including active photocontrol via the introduction of azobenzene moieties. Active control over the folding and self-assembly of β-rich structures is of much interest as well, not only as a tool for the study of natural peptides and proteins, but also as a way to control assembly and (bio)activity of materials based on the β-strand structure.[4, 5]

As discussed in **Chapter 4**, using light as a method of structural control has the advantage of spatial and temporal resolution in combination with biocompatibility, all of which are desirable properties for biomaterials. Photocontrol over β-dominant structures was first demonstrated by the groups of Hilvert and Renner, who independently worked on β-hairpins incorporating azobenzene turn motifs.[6, 7] Both groups used [3-(3-aminomethyl)-phenylazo]phenylacetic acid (AMPP), an asymmetric azobenzene linker, as a photoswitchable turn motif. The *cis* isomer of AMPP is used to position two pentamer peptide sequences at an appropriate distance for hydrogen bond formation, mimicking a β-hairpin, where the *trans* isomer has the wrong geometry to form this structure (**Scheme 6.1A**). This initial research was focussed on gaining understanding over the structure of hairpins and to serve as a model for their folding that could be studied on an ultra-fast timescale.[8-10]

The use of this AMPP linker has been extended to amyloid-forming peptides, demonstrating control over intermolecular self-assembly.[11] The formation of amyloid structures is initiated by protein misfolding resulting in a β-hairpin.[12] This hairpin motif acts as a nucleation point for other proteins, eventually leading to formation of amyloid fibrils. Incorporation of the AMPP linker in the amyloid β-peptide $A\beta_{1\text{-}42}$ yielded control over the tendency to form hairpins via

photoisomerization, with a transition to the *cis* isomer resulting in amyloid fibril nucleation and altered *in vitro* cytotoxicity.[13, 14] Although AMPP introduces photoswitching in β-hairpins, its use outside of model systems has been limited since it can only be used in small, synthetic systems with hairpin domains that are suitable for substitution with the photoactive moiety.

In **Chapter 5** of this thesis the ability of azobenzene-based amino acids to control the folding of coiled-coil peptides was demonstrated; showing that a single amino acid modification can have a significant effect on coiled-coil binding strength. The *trans* to *cis* transition of the azobenzene changes the polarity of the diazene bond, resulting in a destabilization of the hydrophobic coiled-coil interface. We hypothesize that this mechanism of action extends to β-sheet structures, as illustrated in **Scheme 6.1B**, if they self-assemble to form a hydrophobic domain. Specifically, the introduction of phenylazo-phenylalanine (**APhe**), a light-switchable derivative of phenylalanine, is a logical modification of phenylalanine-rich β-sheet domains for the introduction of photoresponsive self-assembly and activity.

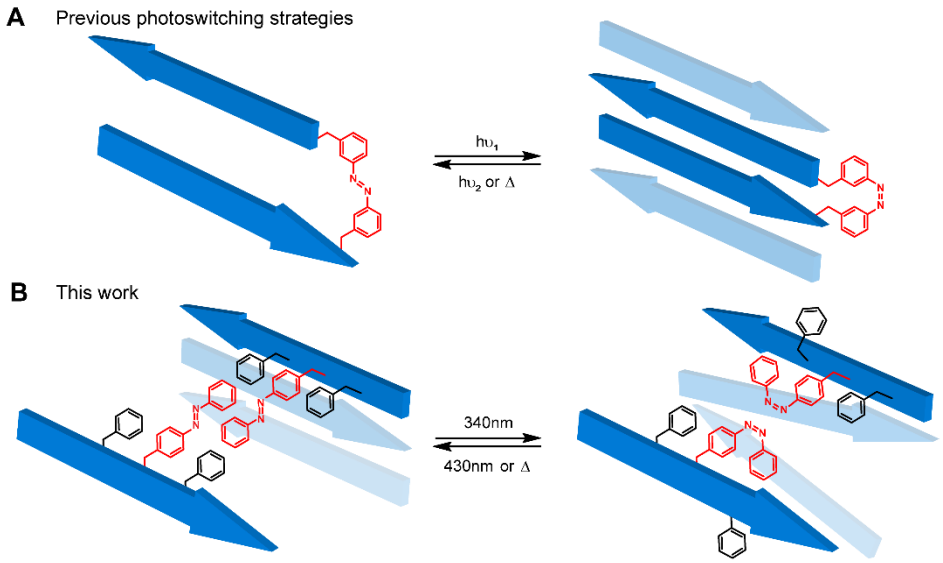

Scheme 6.1: Previous work demonstrating light activated β-hairpin self-assembly (A) and the method investigated in this chapter for photocontrol of β-sheet self-assembly through disruption of the hydrophobic domain (B). Hairpin photocontrol makes use of an azobenzene crosslinker to connect two β-strand sequences, and alter their proximity by isomerization. The strategy in this chapter uses **APhe**, a light-active derivative of phenylalanine, to control self-assembly of β-strand hydrophobic domains.

Inspired by the work on β-sheet peptide assembly and self-replication in the group of G. Ashkenasy,[15, 16] the β-sheet forming peptides studied in this chapter are based on the $(EF)_n$ repeat sequence. This peptide belongs to a family with the general sequence $(XFXF)_n$, where *X* is a polar amino acid, and peptides of this family readily form β-structured self-assemblies.[17] With this alternating amino acid sequence, all hydrophobic side chains are on the same face, resulting in formation of cofacial β-sheet bilayers with all hydrophobic amino acids in the interior of the bilayer.[18] These cofacial β-sheets are comparable to the amyloid cross-β structure,[19, 20] and this class of peptides is often used as a model system for amyloid self-assembly.[21, 22] Peptides based on the $(XFXF)_n$ sequence have been observed to form β-fibres, helical ribbons or tapes and amyloid-like aggregates.[18, 22-24] These larger structures are all based on the same cofacial β-sheet structure repeating in different axes, and can be selected for by alteration of amino acid composition, sequence length and amino acid chirality.[22, 24-26] Substituting phenylalanine with large naphthalene and naphthalene diimide moieties was also well tolerated in these peptides,[27, 28] indicating that incorporation of **APhe** is feasible. For this study, peptide 2 (**Pep2**) from the previous work of Rubinov *et. al.*[16] was prepared, in addition to analogues where a single phenylalanine was substituted by **APhe**. Control over peptide structure could be achieved via azobenzene photoisomerization which resulted in altered self-assembly characteristics. As a proof of concept, modified variants containing histidine residues as catalytic sites were prepared, and photoisomerization was shown to affect organocatalytic activity.

6.2 Results and Discussion

Fmoc-protected **APhe** (**1**, **Figure 6.1A**) based on L-phenylalanine was synthesized according to literature procedures for use in solid phase peptide synthesis (SPPS).[29] A detailed description of the synthesis can be found in **Chapter 5** of this thesis. Isomerization characteristics of **1** in acetonitrile were characterized via liquid chromatography (LC) and showed that in the dark **1** was over 96% in the *trans* configuration (see **Figure 6.1B** and **Figure 6.1C**). Isomerization to the *cis* isomer was performed most effectively using 340 nm light, yielding 90% conversion to *cis*, with a thermal half-life at 20 °C of 27.2h (**figure 6.1D**). Light with a higher wavelength yielded predominantly the *trans* isomer, with no difference observed using wavelengths between 375 nm and 450 nm. Illumination of samples at thermal equilibrium with 435 nm light yielded the same isomeric ratio as samples pre-illuminated with 340 nm, showing these are the photostationary states of the

azobenzene. Up to 81% of the *trans* isomer could be achieved using wavelengths of light between 385 nm and 450 nm, which is less than before illumination, and limits the effect of switching over multiple cycles to approximately 70% of what would theoretically be possible if the azobenzene could be cycled between exclusively the *cis* and *trans* isomers.

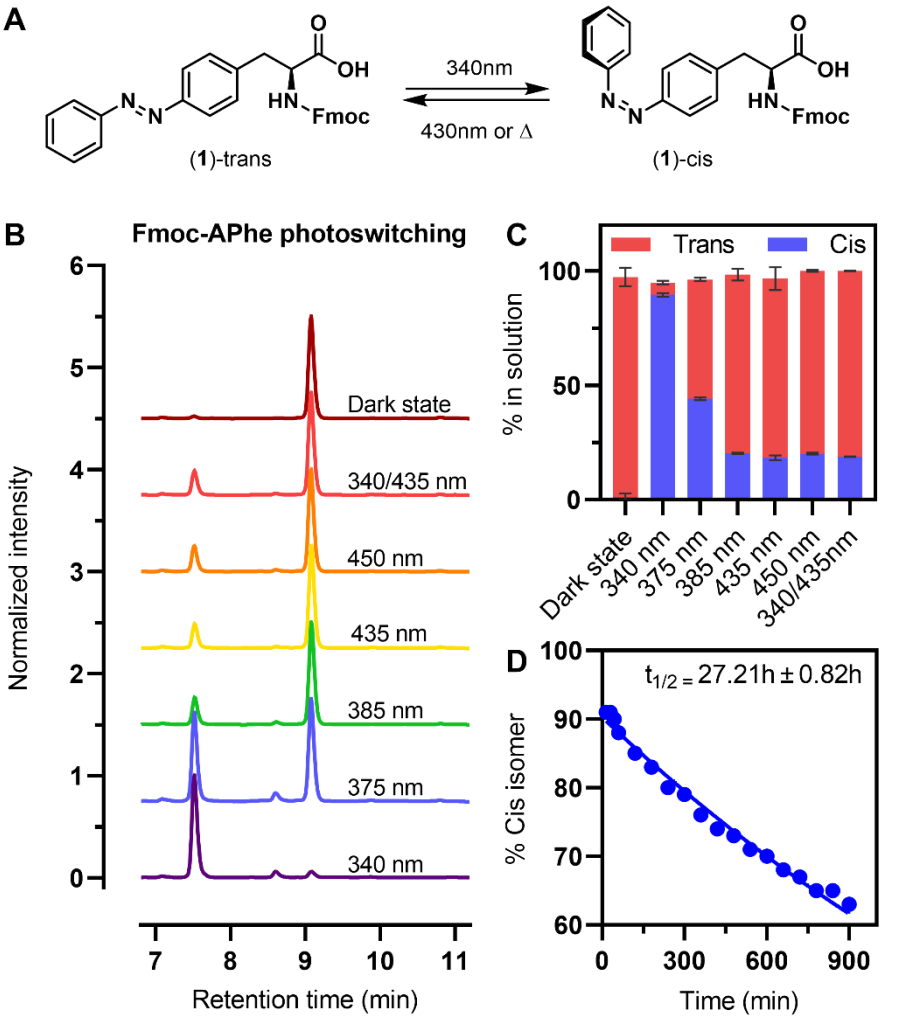

Figure 6.1: Structural differences between the *cis* and *trans* isomers of Fmoc-APhe (A). Liquid chromatography spectra of **1** when illuminated with different wavelengths of light (B), percentage of *cis* and *trans* isomers in solution for the different photostationary states derived from their LC Spectra (D), and thermal relaxation of the *cis* isomer of **1** (C). The isomerization and relaxation studies were performed at 20 °C [**1**]= 200 µM in MeCN. Error bars show differences for 3 repeat measurements.

Peptide design and structural analysis

The β-sheet forming peptide **Pep2** (**Figure 6.2**) was modified with **APhe** by replacing a single phenylalanine at position 2 (**P2**) or position 6 (**P6**) to probe the ability to photoswitch these peptides. Because the **APhe** moiety is larger in size then phenylalanine, any beta-sheet domain will have to change shape to allow complete incorporation of the amino acid into the hydrophobic core. This change in shape is expected to be different depending on the location of **APhe**, and should therefore result in different self-assembly dynamics.

Self-assembly of **Pep2** and its derivatives was first assayed via circular dichroism (CD) spectroscopy to observe under which conditions β-sheet assembly occurred. Peptides rich in β-structures can be classified by the alignment of adjacent strands (parallel or anti-parallel) and the presence of twist within the β-strand, all of which have their own distinguishable CD absorption bands.[30] **Pep2** showed a low CD signal when dissolved in phosphate buffer at a 100 μM peptide concentration, with no characteristic bands for any type of β-structure. Because the presence of salts in solution increases the hydrophobic effect, and can aid self-assembly by the formation of salt bridges between charged amino acid side chains, the dependence of folding on salt concentration was assayed. Adding Na_2SO_4 to the buffer to increase peptide-peptide interactions caused a change in structure, with two negative absorption bands appearing; a sharp band at 202 nm and a broad band with a minimum at 218 nm (**Figure 6.2, left**). Titration experiments showed a sigmoidal dependence of the CD signal on the salt concentration with a mid-point ($f_{1/2}$) at 0.85 M Na_2SO_4.When the salt concentration was kept constant at 1 M Na_2SO_4, an initial linear dependence of structure on peptide concentration was observed with a maximum at approximately 150 μM (**Figure S6.1**).

Peptide variants **P2** and **P6** showed similar spectral shapes to **Pep2**, in the absence of salt, but with more intense minima. Both variants showed signal increase upon Na_2SO_4 addition, with clear differences observed between the dark and light (illuminated with 340 nm) state of the peptides. Peptide **P2** showed similar absorption peaks as **Pep2** when salt was added, with minima located at 204 and 216 nm. Lower absorption minima were observed for **P2**, indicating a higher degree of folding, but in a more irregular manner as suggested by lower separation between the peaks. The spectrum of **P6** shows a single clear absorption minimum at 225 nm, with the absorption rising sharply below that wavelength, suggesting a strong absorption maximum between 195-200 nm. This spectrum is consistent with

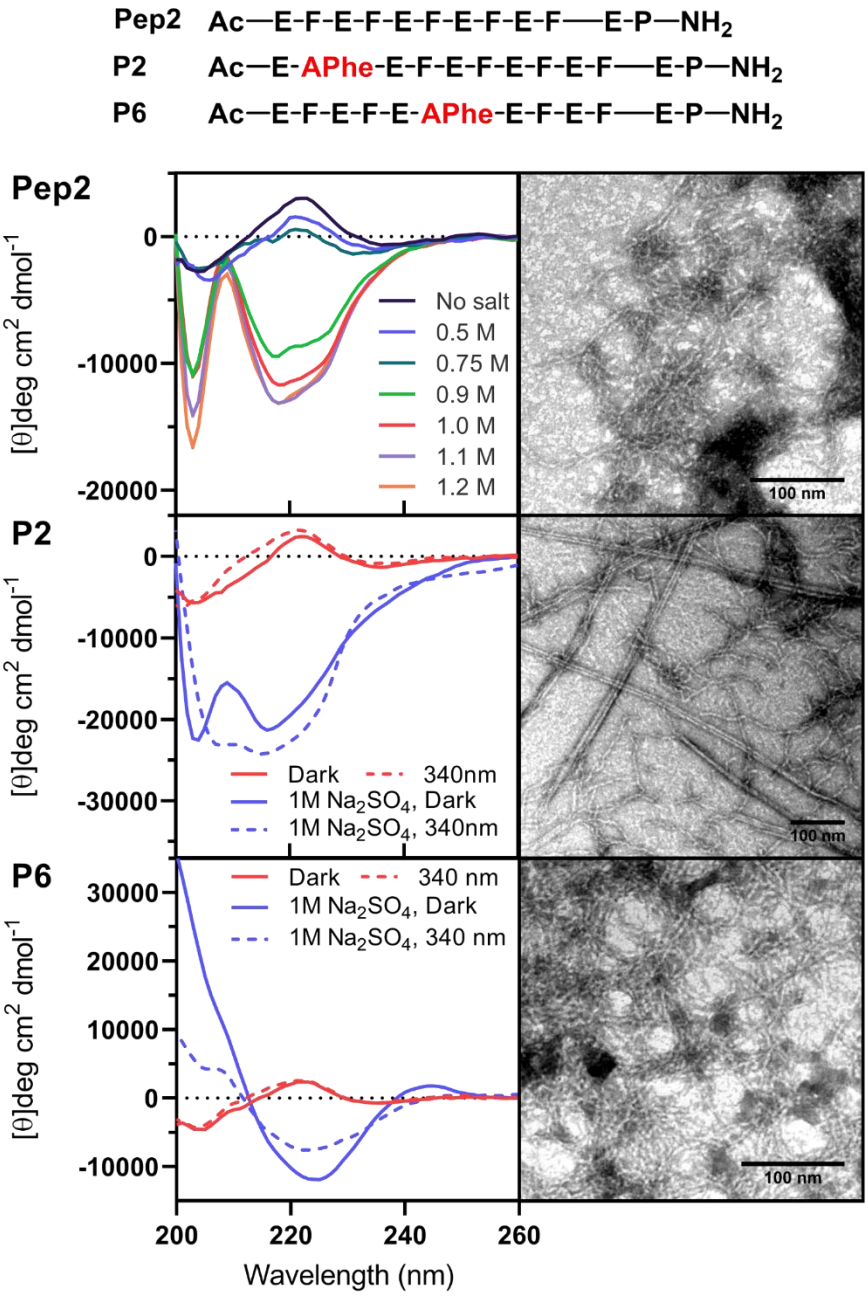

Figure 6.2: Schematic structure of the peptide variants prepared for photoswitching studies (top), their solution CD spectra with varying levels of Na_2SO_4 (bottom left) and TEM images of their formed structures (bottom right). CD spectra were recorded at 100 µM peptide concentration, with 10 mM PB at pH 7.2.

that of left-twisted anti-parallel β-sheet peptides, with the maxima slightly blue shifted. Upon irradiation of the **APhe** containing peptides with 340 nm light, the CD spectra changed, indicative of structural rearrangement in the peptide assembly. The **P2** variant has a slightly stronger absorption minima at 216 nm, with the two absorption minima observed for the dark state broadening to the point that they are difficult to distinguish. The **P6** variant shows a general decrease in signal strength upon irradiation, with a less intense and blue shifted absorption band, and a less steep increase in signal at the lower wavelengths. Other salts were also tested for their effects on peptide folding, with the largest effect observed for Na_2SO_4 (**Figure S6.2**), which was used for all further experiments.

The CD spectra show β-sheet structures for all three peptides when salt is present in solution, which is the main mechanism for their self-assembly into peptide fibres. To characterize their self-assembly, samples were imaged using transmission electron microscopy (TEM), revealing the presence of long fibrillar structures for all three peptides (**Figure 6.2, right**). Samples of **P6** contained fibres with a width of 5.7 ± 0.5 nm, which is comparable to the thickness of fibres observed for the parent peptide **Pep2** (5.5 ± 0.4 nm). Thicker and less uniform (7.2 ± 1.0 nm) fibres were observed for **P2**, which additionally showed larger, linear assemblies that appear to consist of 2 (double) or more (multiple) fibres bundled together. Analysis of the larger assemblies in the **P2** sample (representative image shown in **Figure S6.3**) shows a repeating pattern with spacing of the same size as single fibres. An overview of fibre thickness is given in **Figure S6.4** and **Table S6.1**. These results suggest that peptide **P2** is capable of forming peptide fibres, similar to the other two peptides, although with a different overall structure since the CD signal of the peptide is quite different and fibre oligomerization is observed. This polymerization of **P2** peptide fibres suggests that the ends of the β-sheet, where the peptide termini are located, are not as stable as for the other two variants. The **APhe** moiety is relatively large and more hydrophobic compared to phenylalanine, and when placed at the termini such as in peptide **P2** likely results in rearrangement of the fibre structure to minimize interactions between the azobenzene and the aqueous environment. Aggregation of multiple fibres at the terminal ends would allow the azobenzene to be shielded from the environment by the neighbouring fibre, resulting in a more classical β-sheet structure.

Because a characteristic dependence of peptide folding on the concentration of dissolved salts was observed for peptide **Pep2**, titrations were performed with its **APhe** substituted derivatives. The light irradiated (*cis* dominant) and thermally

equilibrated (*trans* dominant) states of **P2** at 100 µM showed different behaviours, with the *trans* dominant sample folding at a lower salt concentration ($f_{1/2}$ = 0.66 M vs 0.79 M, **Figure 6.3** and **Figure S6.5**) but the irradiated state shows a stronger signal at 218 nm. A different behaviour was observed for **P6**, where the dark state showed both a lower midpoint ($f_{1/2}$ = 0.45 M vs 0.58 M, **Figure 6.3** and **Figure S6.6**) and a higher degree of overall folding. Comparing the response to changes in Na_2SO_4 concentration for all three peptides shows that **APhe** modifications at position 6 has the largest effect on self-assembly, lowering the transition point for folding by 47% with respect to **Pep2**. Modification at the terminus, as seen in **P2**, also reduced this transition point by 22%, showing that the **APhe** amino acid has a favourable effect on peptide self-assembly. The transition point for salt-dependent

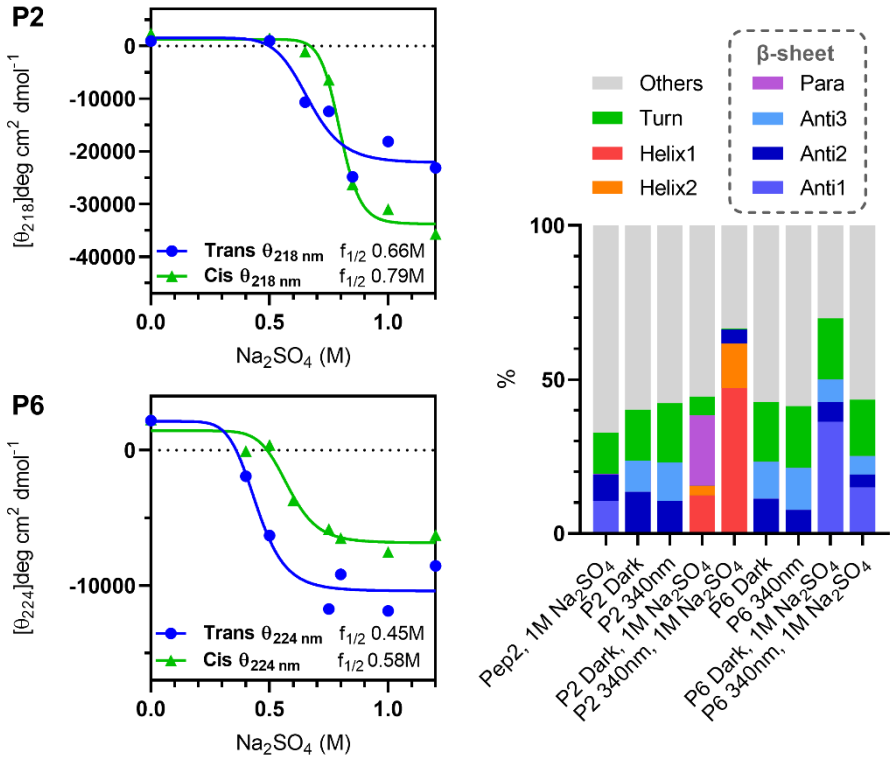

Figure 6.3: Structural dependence of peptides **P2** and **P6** on the concentration of sodium sulphate demonstrated via CD titrations (left), and structural deconvolution of CD spectra discussed in this chapter using the BeSTSel web server (right).[31] CD titrations were performed at 100 µM peptide in 10 mM PB, complete spectra can be found in **Figure S6.5** and **Figure S6.6**. Figure legend: Anti1 = left-twisted β-strand; Anti2 = relaxed β-strand; Anti3 = right-twisted β-strand; Helix1 = regular α-helix; Helix2 = distorted α-helix; Para = Parallel β-strand.

self-assembly was different between the *cis* and *trans* state for both novel peptides, showing that these isomers have distinct self-assembly behaviours.

To better understand the structural components of the β-sheet forming peptides discussed in this chapter, the CD spectra in **Figure 6.2** were analysed using the BeStSel web server, which was specifically designed to deconvolute CD spectra of β-structure rich proteins.[30, 31] The results of this analysis are shown in **Figure 6.3** (right) and **Table S6.2**. Both **P2** and **P6** show a mixed structure, consisting of relaxed and left-twisted β-strands, and turn motifs when no salt is present. With 1 M Na_2SO_4 **P6** shows increased folding (70% folded structures over 43% with no salt), dominated by right-twisted β-strand motif. Upon *trans* to *cis* isomerization of **P6**, the amount of folded structures is reduced by 26%, predominantly via loss of the right-twisted β-strand motifs (21% less). Analysis of peptide **P2** with salt shows a structure dominated by parallel β-strand motifs in the dark state, combined with some α-helical structures. Upon light irradiation of **P2,** helical structures become recognized as the dominant structural fold. This originates from the two observed absorption minima at 218 nm and 202 nm and an apparent absorption maximum below 200 nm, which is similar but blue shifted from what one would expect for a helical peptide. However, the amino acid sequence should not be predisposed to form helical structures,[2] and the peptide is based on a known β-sheet forming sequence. Since the sequence of **P2** is not encountered in nature, it can adopt structures unfamiliar to the BeStSel algorithm, which was trained on solved protein structures. This is also supported by the lack of β-sheet structure attributed to **Pep2**, a known anti-parallel β-sheet forming peptide, by the BeStSel algorithm. Furthermore, the absorption peaks observed for **P2** resemble previously reported spectra for β-sheet forming peptides with the $(KFKE)_n$ repeat sequence.[24, 32] Because of this similarity in the CD spectra of **P2** to previously reported β-sheet peptides and its ability to form fibres in solution with a similar dimension to those of **Pep2** and **P6**; it most likely forms peptide fibres dominated by β-sheet structures.

Characteristics of fibre formation

The structural analysis via CD spectroscopy shows the dependence of peptide folding on concentration and solutes, which is related to the self-assembly of peptides into larger structures, but does not provide any insight into self-assembly. To further investigate the self-assembly into β-sheet fibres the critical aggregation concentration (CAC) was determined using dynamic light scattering (DLS). Plotting the observed count rate in DLS versus the peptide concentration shows two distinct

domains; one at lower concentration where the count rate did not increase significantly, and a domain at higher concentration where the count rate increased rapidly (**Figure 6.4A**). The intersect of these two domains is defined as the CAC for that condition (CAC data for all peptides and conditions can be found in **Table S6.3**). Peptide **P2** and **P6** both showed a low CAC with 1 M Na_2SO_4 in solution, of 6 and 11 µM respectively, which increased when samples were irradiated with 340 nm light. The CAC of **P2** increased 4.8 times after irradiation (**Figure 6.4A** left) and the CAC of **P6** increased by 1.8 times (**Figure S6.7**). The lower difference between the light and dark state was assumed to relate to the difference between the salt

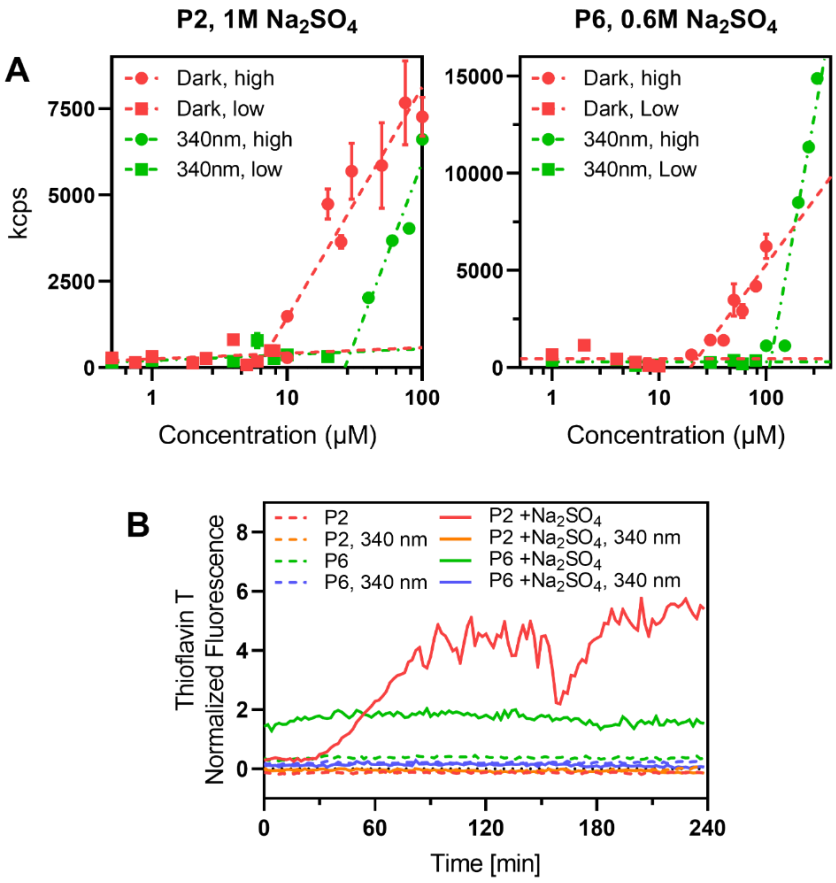

Figure 6.4: Light scattering count rate dependence on the concentration of peptides **P2** and **P6** for determination of CAC (A) and thioflavin T fluorescence used to observe the kinetics of beta-sheet fibre assembly at [peptide] = 100 µM (B). Fluorescence was recorded at 490 nm and normalized to the fluorescence of Thioflavin T with no peptides in solution, which is set to 0. Fluorescence samples contained [ThT] = 100 µM and [Na_2SO_4] = 1 M if present.

dependence observed via CD spectroscopy. Therefore, the experiment was repeated for **P6** at a reduced concentration of 0.6 M Na_2SO_4, resulting in a 5-fold increase in CAC from 22 to 109 µM (**Figure 6.4A**, right). This indicates that the CD titration experiments relate well to formation of self-assembled aggregates.

To investigate the type and kinetics of self-assemblies formed by the peptides, Thioflavin T (ThT) was used as a fluorescent probe. The fluorescence behaviour of ThT is dependent on its environment; it specifically known to bind to β-sheet rich protein domains, resulting in a large increases in fluorescence intensity and a shift in emission wavelength.[33, 34] Because of this property, it has been used in the study of amyloid fibres and plaques.[35] Kinetic experiments were performed with peptides **P2** and **P6** at 100 µM adapted to dark conditions or irradiated with 340 nm light, in PB with and without 1 M Na_2SO_4. Only the samples prepared with dark adapted peptides and containing 1 M Na_2SO_4 showed a significant increase in ThT fluorescence. Peptide **P2** initially shows no fluorescence increase, but after 30 minutes a steady rise in the signal observed, which evens out at 5-fold more fluorescence after 4 hours. In contrast, **P6** showed an immediate increase, stabilizing around a 2-fold increase in fluorescence during the remainder of the experiment.

Overall, we observed different assembly kinetics for the two azobenzene containing peptide variants; fast assembly for **P6** and nucleated self-assembly for **P2**. The fluorescence of **P6** is increased from the start of the experiment (about 30 seconds after mixing) and quickly reaches a plateau where ThT fluorescence intensity does not change. In contrast, a lag phase is observed at the start of the experiment for **P2**, followed by an increase in fluorescence that keeps going through the remainder of the experiment. This suggests the requirement for a nucleation point or β-sheet seed that initiates the self-assembly process. This nucleated assembly is very similar to what has been observed for amyloid-like aggregates of insulin, a known model system for amyloidogenic proteins.[35] This comparable kinetic mechanism strengthens the idea that the fibres formed by **P2** form β-sheet dominated structures similar to amyloids. With no salt in solution both peptides were unable to form these larger structures, mirroring the observed effect of salt on β-sheet structure observed in CD experiments. No increase in signal was observed if peptide samples were pre-irradiated with 340 nm light, showing that the effect of **APhe** isomerization observed in CD and CAC experiments is large enough to control intermolecular self-assembly.

Cryo-EM analysis of P6

The solution-based experiments show that peptide self-assembly is dependent on both peptide concentration and dissolved solutes. This raises the question; how well do the peptide fibres observed with TEM in **Figure 6.2** represent the structure of the peptides observed in solution? The TEM samples of these peptides are prepared from high-concentration peptide stock solutions containing no added Na_2SO_4, which seems essential for self-assembly. Furthermore, the drying of the sample and negative staining with uranyl acetate might influence their morphology in a manner which is difficult to predict. Therefore, peptide **P6** was also investigated via cryogenic electron microscopy (cryo-EM), shown in **Figure 6.5**. Long (>100 nm) fibres were observed with a diameter of 4.5 ± 0.9 nm, which is comparable in size to those observed in TEM (5.7 ± 0.5 nm). The slight (not significant) difference in average size can be explained by the drying and staining procedures discussed above.

Previous use of peptides with $(EF)_x$ repeat motifs showed formation of self-assembled structures in MD simulations consisting of two antiparallel β-sheet monolayers oriented antiparallel to each other,[36] similar to the previously discussed cross-β structure. A model of **P6** was prepared assuming this structure, and is shown in **Figure 6.6**. A cross-section of this structure has a width of 4.6 nm (**Figure S6.8**), which reflects the observed fibre width in TEM and cryo-EM. Therefore, we conclude that the structure of **P6** is likely the discussed double antiparallel β-sheet, with the width of the fibre equalling the length of a single peptide chain.

Introduction of catalytic activity

The light-controlled self-assembly of beta-sheet fibres of peptides **P6** and **P2** might enable control over structure-related activity of these peptides. variants of **P6** were synthesized containing a histidine (His) in its sequence. Histidine has a nucleophilic nitrogen with a pK_a between 6 and 7 depending on its environment,[37] allowing it to function both as a proton transfer group as well as a nucleophilic catalyst. In various self-assembled systems, introduction of His moieties has been shown to result in organocatalytic activity of self-assembled materials.[38-40] Peptide **P6** was chosen over **P2** because it self-assembles at a lower salt concentration, and has only been observed to self-assemble into one structure which is highly folded as an anti-parallel β-sheet.

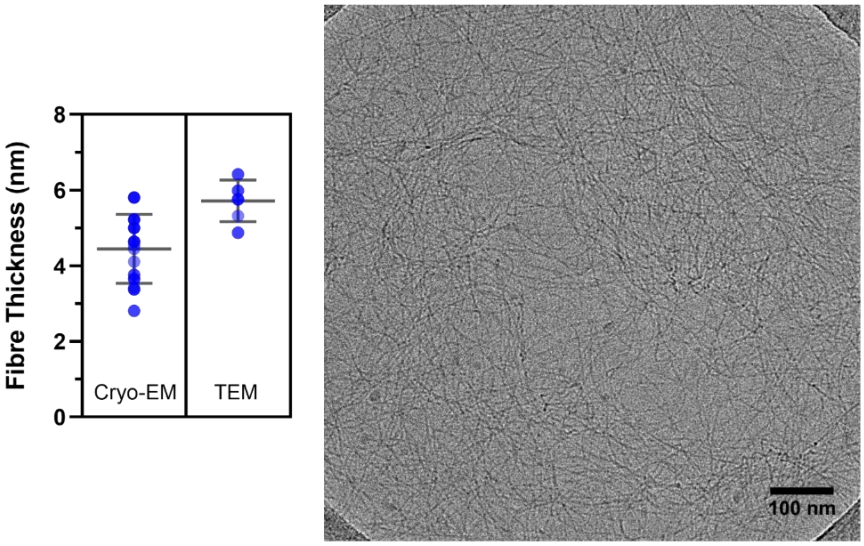

Figure 6.5: Cryo-EM images of fibres formed by peptide **P6** in solution (right), and distribution plot of the measured fibre width in nm (left) for both cryo-electron microscopy and transmission electron microscopy. Scale bar indicates 100 nm, and the image was recorded at 36K magnification, yielding a nominal pixel size of 2.8 ångström (Å).

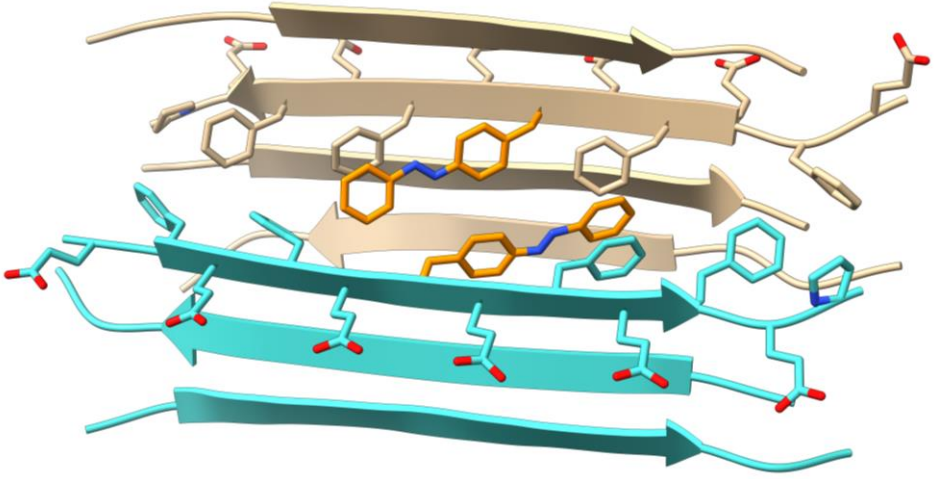

Figure 6.6: Model showing **P6** assembled into a double antiparallel β-sheet structure, which is the hypothesized structure for the peptide fibres observed under TEM and Cryo-EM. Two opposing strands are coloured separately for clarity and have their side chains displayed, with the **Aphe** moiety coloured orange. The remaining strands are displayed as a cartoon, showing the direction of the β-sheet fibre. Fibre model was prepared using the UCSF chimera and chimeraX software package.[41, 42]

Two histidine containing variants were prepared, one where a single phenylalanine was replaced by His and a second where a single glutamic acid was replaced by His. These two variants were synthesized to observe the difference in self-assembly and catalysis when the His was placed in a hydrophobic or hydrophilic environment. The resulting peptides were named **P5H-P6** and **P6-P8H**, and are shown in **Figure 6.7**. His substitution was performed close to the azobenzene moiety, as this was expected to maximize the effect of photoswitching on catalysis.

CD spectra of dark-adapted **P5H-P6** show a strong minimum at 206 nm, with a shoulder at 218 nm, indicative of a mixed irregular and right-twisted β-sheet

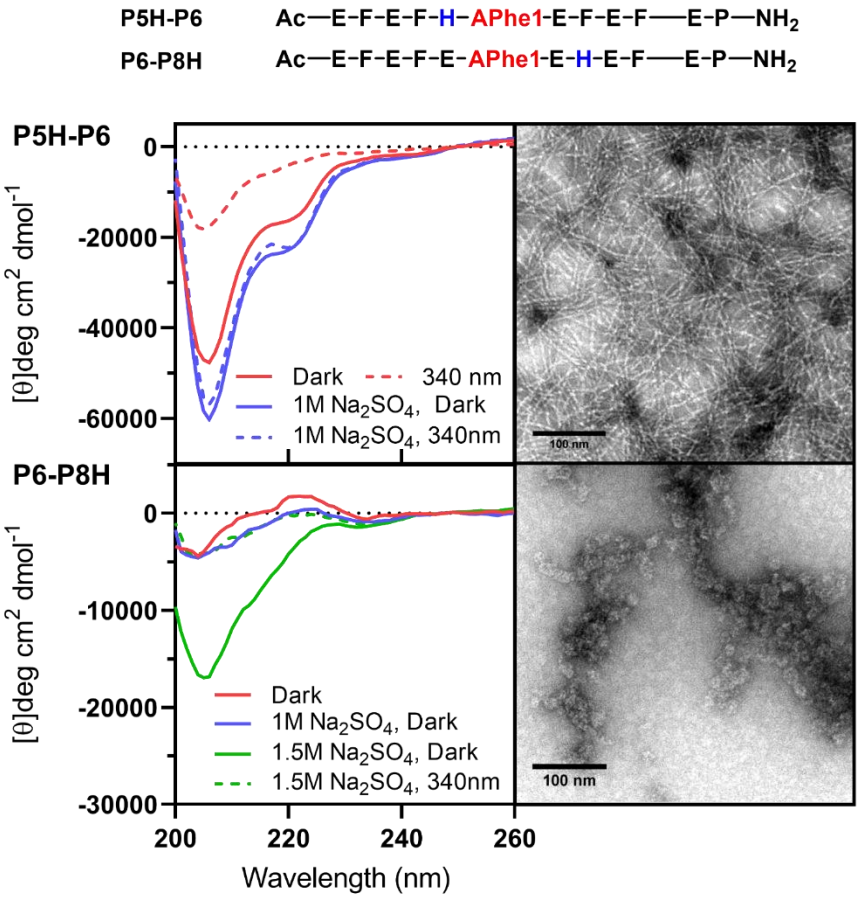

Figure 6.7: Peptide sequences (top), CD spectra (left) and TEM images (right) of histidine-containing peptides. CD spectra were recorded with [peptide] = 100 μM and 10 mM PB. TEM samples were treated with uranyl acetate as a negative stain before imaging, with scale bars indicating 100 nm.

structure. Peak intensity at 206 nm is higher than one would expect for a combination of these two, suggesting the structure might differ from both of these.[30] Isomerization of the sample with 340 nm light results in a decrease in overall folding, with a 60% reduction of the signal at 206 nm and 70% reduction of the signal at 218 nm. CD spectra of **P5H-P6** containing added Na_2SO_4 showed an overall increase in signal strength at both wavelengths, but only marginal differences between the dark adapted and 340 nm photostationary state. From 200 mM Na_2SO_4 and higher, no differences between the two states could be observed (**Figure S6.9**). Although the CD spectra and response to added salt are very different from the **P6** parent peptide, TEM imaging still shows fibre formation, with a similar fibre width (6.35 ± 0.39 nm, **Figure S6.4**) to **P6**. The opposite is observed for substitution of a phenylalanine with histidine in peptide **P6-P8H**, which did not assemble into fibres (**Figure 6.7**). Instead, spherical aggregates were observed with no apparent (internal) structure. In CD spectroscopy, **P6-P8H** shows a weakly folded signal until the salt concentration has been increased to 1.5 M Na_2SO_4, which displays a broad absorption peak with a minimum at 205 nm. At the high salt concentration there is a clear difference between the spectra of the dark adapted and 340 nm irradiated samples, with the irradiated sample again showing weak folding. An exact secondary structure cannot be assigned to this absorption peak in isolation, and the broadness of the peak suggests that it there might be some flexibility in its structure. Both histidine-containing peptides show different CD spectra from **P6**, but they are comparable in shape to previous reported CD spectra on peptides with the repeat sequence $(FKFE)_n$, which self-assemble as antiparallel cofacial β-sheet fibres.[22, 24]

The two histidine-containing peptides were tested for catalytic activity in the ester hydrolysis of *para*-nitrophenylacetate (*p*NPA), a common marker for hydrolysis because of the strong absorbance of the *para*-nitrophenol product.[43, 44] Peptides were tested for catalytic behaviour at a concentration of 300 μM to increase signal (self-assembly characteristics as studied by CD were comparable between 100 and 300 μM, **Figure S6.10**). Both peptides showed an increase in hydrolysis, with **P6-P8H** showing the largest substrate conversion (**Figure 6.8A**). The rate of hydrolysis with **P6-P8H** was dependent on the peptide concentration, demonstrating its function as a catalyst, and similar catalytic turn-over frequencies were found at 100 μM (0.068 h^{-1}) as at 300 μM (0.078 h^{-1}) of peptide. Isomerization of **P6-P8H** with 340 nm light resulted in a 34% reduced reaction rate, showing the catalysis can be influenced by the **APhe** photoswitch adjacent to the histidine. Because the histidine

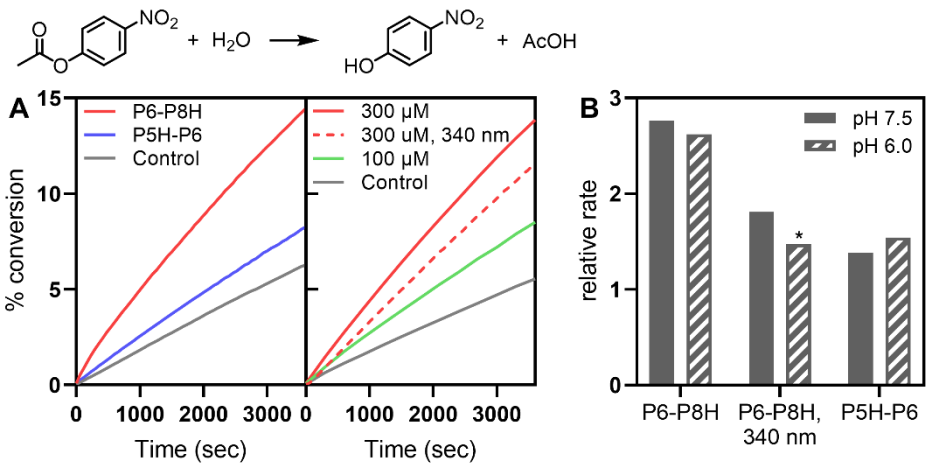

Figure 6.8: Catalytic effect of His-containing peptides on the rate of *p*-nitrophenylacetate hydrolysis. Kinetic experiments comparing the two catalytic peptides (A, left) and the effect of concentration and 340 nm illumination on peptide **P6-P8H** (A, right). Initial rate of hydrolysis relative to background rate (B), asterisk indicates the rate was calculated over the entire experiment. [pNPA] = 200 µM, [peptide] = 300 µM at 25 ˚C and in pH 7.5 phosphate buffer unless noted otherwise. Kinetic experiments for pH 6.0 can be found in **Figure S6.11**.

protonation state was theorized to affect catalytic rates, the experiments were repeated at pH 6.0, with no effect on the relative rate of ester hydrolysis (**Figure 6.8B**). Peptide **P6-P8H** showed the best catalytic activity for the hydrolysis of pNPA, and its activity could be controlled by **APhe** isomerization, reducing its TOF by 54% by irradiation with 340 nm light. The mechanism through which catalytic activity is affected is not yet clear, since it does not show characteristic β-sheet assembly as the other peptides do.

6.3 Conclusions and outlook

The photoswitchable amino acid **APhe** was successfully incorporated in phenylalanine-based β-sheet forming peptides in the centre of the sequence or close to the terminus. Both modified positions resulted in peptides that self-assembly as β-sheet dominant structures in the presence of Na_2SO_4. Both peptide structure and CAC are dependent on the salt concentration, and effect of salt on folding was related to the effect on CAC. TEM images showed peptide fibres for both variants, with peptide **P2** also showing fibrillar structures multiple times the fibre width. Soluble fibres were observed for peptide **P6** via cryo-TEM, and showed a fibre width consistent with self-assembly of the peptide as a cofacial β-sheet structure. Irradiation with 340 nm light resulted in isomerization of the azobenzene

to dominantly *cis*, and resulted in a loss of structure as observed via CD, and a 5-fold reduction in the observed CAC. Kinetic experiments using Thioflavin T showed an initial lag period for **P2**, suggesting a cooperative assembly mechanism, and both switchable variants did not show increased signal when isomerized to the *cis* conformation. From this we conclude that **APhe** can be used to control the self-assembly of β-sheet peptides, with the most effective control occurring if it is placed in the centre of the β-sheet domain. Positioning of **APhe** at the termini of the peptide does allow for photocontrol, but also leads to oligomerization of the peptide fibres in solution.

Histidine containing variants of **P6** were prepared and tested as a catalyst for ester hydrolysis. The histidine significantly altered the self-assembly of the peptides, which no longer adhered to the salt-induced self-assembly observed for the parent peptide **P6**, and resulted in non-fibrous structures when substituting a phenylalanine in the case of **P6-P8H**. Both peptides showed a rate of ester hydrolysis above background, with the largest increase in rate observed for **P6-P8H**. The reaction rate could be reduced via isomerization with 340 nm light, showing **APhe** isomerization can be used to control the catalytic activity.

6.4 Methods

Fmoc-protected amino acids were purchased from Novabiochem (Amsterdam, The Netherlands). Acetic anhydride (Ac_2O), acetonitrile (MeCN), dimethylformamide (DMF), piperidine, pyridine, trifluoroacetic acid (TFA) and tetrahydrofuran (THF) were purchased from Biosolve (Valkenswaard, The Netherlands). Oxyma was purchased from Carl Roth (Karlsruhe, Germany). N,N'-Diisopropylcarbodiimide (DIC), 1,2-Bis(2-mercaptoethoxy)-ethane (EODT) , 1-[Bis(dimethylamino)methylene -]-1H-1,2,3-triazolo[4,5-b]pyridinium 3-Oxide Hexafluorophosphate (HATU), and Thioflavin T were purchased from Sigma Aldrich (Zwijndrecht, The Netherlands). Chloroform, dichloromethane (DCM), ethyl acetate (EtOAc), ethanol, diethyl ether (Et_2O) and pentane were supplied by Honeywell (Meppel, The Netherlands). All reagents were used as purchased. Ultrapure water was purified using a Milli-Q™ purification system from Millipore (Amsterdam, The Netherlands). A detailed description of the synthesis of **1** can be found in **chapter 5** of this thesis.

Peptide synthesis was performed via Fmoc-based SPPS, on a CEM liberty blue microwave-accelerated peptide synthesizer. Peptides were prepared on a 0.05 or 0.1 mmol scale using Tentagel HL resin (0.39 mmol/g), using 5 equivalents each of

amino acid, Oxyma pure and DIC as coupling reagents at 90 °C for 4 minutes. Deprotection was achieved with 20% piperidine in DMF heated to 90 °C for 1 minute. Between deprotection and peptide coupling 3 DMF washes were performed, with a single washing step between the coupling and deprotection steps. Amino-acid **1** was coupled manually to reduce the required equivalents, using 2.5 equivalents of **1**, 2.5 equivalents of HATU, and 5 equivalents DIPEA in DMF for 2-3 hours. After the last Fmoc deprotection, the N-terminus was acylated using 5 mL/mmol each of Ac_2O and pyridine in DMF, for 5 minutes. To eliminate potential light absorption, the N-terminus of **pep2** and derivatives was acetylated instead of capping with 4-acetaminobenzoic acid as previously reported.[16] The resin was washed 3 times with DMF, MeOH and DCM followed by drying under a continuous air flow. Cleavage of peptide was achieved with TFA (5 mL) containing 2.5% water and 2.5% TIS for 1 hour, followed by precipitation in 1:1 C_5H_{12}/Et_2O. The precipitate was collected via centrifugation (4000 rpm, 10 minutes), the organic layer removed and the product resuspended in water for purification or lyophilization.

Peptides were purified using reverse-phase HPLC on a Shimadzu system consisting of two KC-20AR pumps and an SPD-20A or SPD-M20A detector fitted with a Phenomenex Kinetix Evo C18 column. A linear gradient from 2-35% MeCN in water containing 0.1% NH_3 as buffer in both phases, at a flow rate of 12 ml/min. Collected fractions were checked via analytical HPLC, pooled and lyophilized. LC-MS analysis was performed with a Thermo Scientific TSQ quantum access MAX mass detector connected to an Ultimate 3000 liquid chromatography system fitted with a 50x4.6 mm Phenomenex Gemini 3 μm C18 column.

Analytical HPLC was performed using a Shimadzu Prominence-*i* LC-2030C 3D system fitted with a Phenomenex Kinetix Evo C18 column. For quantification of **1** photoswitching, a linear gradient of 10-90% MeCN in water containing 0.1% TFA. Peptide purity was confirmed with analytical HPLC using a gradient of 5-50% MeCN in water and containing with 10 mM NH_3 as buffer.

CD spectra were recorded on a Jasco J-815 CD spectrometer fitted with a Peltier temperature controller. Spectra were record in a 1 mm quartz cuvette at 20 °C, unless otherwise specified. Spectra were recorded between 190 and 280 nm with 1 nm intervals, at a scan rate of 100 nm/min with 5 subsequent spectra averaged for accuracy. The mean residue molar ellipticity (θ, deg cm^2 $dmol.res^{-1}$), was calculated using equation 1:

$$[\theta] = (100 * [\theta]_{obs})/(c * n * l) \quad (1)$$

Where $[\theta]_{obs}$ represents the observed ellipticity in mdeg, *c* represents the peptide concentration in mM, *n* the number of peptide bonds and *l* the path length of the cuvette in cm.

TEM samples were prepared on carbon/formvar coated 200 mesh copper grids by the addition of a drop of 0.5 mM peptide solution (containing 10 mM phosphate buffer). After 30 seconds, excess solution was blotted and the grid stained with uranyl acetate (0.25 mg/ml) for less than 10 seconds, and excess liquid removed. The grids were left to air dry completely for at least 2 hours. Measurements were performed on a JEM1400 plus transmission electron microscope operating at 80 kV and fitted with a CCD camera.

Cryo-TEM samples of **P6** (3 µL, 300 µM total concentration) were applied to a freshly glow-discharged Lacey carbon film 200 mesh Cu grid from Electron Microscopy Sciences (Wageningen, The Netherlands). Grids were blotted for 3 s after a 10 s wait at 99% humidity in a Thermo Fisher FEI VitrobotTM Mark III (Landsmeer, The Netherlands). Cryo-EM images were collected on a Talos L120C (NeCEN, Leiden University) operating at 120 kV. Images were recorded manually at a nominal magnification of 36000x yielding a pixel size at the specimen of 2.8 ångström (Å). Images were analyzed using the Fiji software program.[45]

DLS measurements were performed on a Malvern Zetasizer Nano S, using plastic micro-cuvettes. The attenuator was fixed manually at 10, with each experiment consisting of 10 scans of 20 seconds duration. The measurement was repeated 3 times. For each peptide and condition a set of samples was prepared in amber Eppendorf tubes, and left to incubate for a minimum of 2 hours before measurement. The samples were agitated with a pipette just before transferring to the cuvettes. For experiments requiring the *cis* isomer, samples were prepared from stock solutions irradiated with 340 nm, and irradiated again for 3 minutes before the start of the measurement.

UV-Vis spectra were recorded on an Agilent Cary-300 UV-Vis spectrophotometer, at a scanning speed of 200 nm/min with a switchover between the visible and ultraviolet lamp at 350 nm. Samples were measured in quartz cuvettes with a path length of 10 mm, and baseline corrected using a blank sample of the same solvent used for sample preparation. During the measurements, samples were kept at room temperature (20˚C) using an Agilent Cary temperature controller.

Kinetic hydrolysis experiments were carried out on an Agilent Technologies, Cary 60 UV-Vis spectrophotometer. The substrate, *p*NPA was dissolved in acetonitrile (10mM) and the peptide catalysts were dissolved in phosphate buffer (0.1 mM, pH 6.0 or pH 7.5). The experiments were performed with 200 µL samples containing 100 or 300 µM peptide and all solutions were equilibrated at 25 °C for 20 minutes. Reactions were performed in QS quartz cuvettes with a 1 cm path length and equipped with Teflon stoppers (3.5 mL; Starna Analytics). Experiments were performed at 25°C and started by addition of the pNPA stock solution (2 v%), with substrate hydrolysis monitored for 1-4h. As a control, water was added instead of the peptide stock solutions. The following extinction coefficients at 400 nm were used: ε = 1700 M^{-1} cm^{-1} (pH 6.0, 25 °C, 4-nitrophenolate), ε = 16400 M^{-1} cm^{-1} (pH 7.5, 25 °C, 4-nitrophenolate).

Fluorescence experiments were performed in 96-well plates using a TECAN Infinite M1000 Pro microplate reader. For Thioflavin T experiments, fluorescence was recorded every minute, with excitation set at 450nm (± 5nm) and emission at 490nm (± 10nm). All numbers were normalized to the fluorescence of Thioflavin T under the same buffered conditions.

Sample illumination Sample illumination at 340 nm was achieved using a Thorlabs M340F3 Fiber-coupled LED powered by a T-Cube driver at 1000 mA. For all other wavelengths, high-power single chip LEDs were purchased from Roithner Laser (Vienna, Austria) from the H2A1 series. LEDs from Roithner Laser were mounted on an aluminum back plate for heat dissipation, and powered at 350 mA current using a driver built in-house. For illumination the LED was placed parallel to the side of the cuvette at a distance of 5 mm, and centered to the width and height of the sample.

6.5 Acknowledgments

This work benefited from access to the Netherlands Centre for Electron Nanoscopy (NeCEN) at Leiden University, an Instruct-ERIC centre, with technical assistance from Ludovic Renault, Willem Noteborn, Wen Yang and Jamie Depelteau.

6.6 References

1. Rose, G. D.*, et al.* (**2006**) A backbone-based theory of protein folding. *P. Natl. Acad. Sci. USA 103*, 16623-16633.

2. Nick Pace, C., and Martin Scholtz, J. (**1998**) A Helix Propensity Scale Based on Experimental Studies of Peptides and Proteins. *Biophys. J. 75*, 422-427.

3. Xiong, H., *et al.* (**1995**) Periodicity of polar and nonpolar amino acids is the major determinant of secondary structure in self-assembling oligomeric peptides. *P. Natl. Acad. Sci. USA 92*, 6349-6353.

4. Levin, A., *et al.* (**2020**) Biomimetic peptide self-assembly for functional materials. *Nat. Rev. Chem 4*, 615-634.

5. Hauser, C. A. E., and Zhang, S. (**2010**) Designer self-assembling peptide nanofiber biological materials. *Chem. Soc. Rev. 39*, 2780-2790.

6. Aemissegger, A., *et al.* (**2005**) A Photoinducible β-Hairpin. *J. Am. Chem. Soc. 127*, 2929-2936.

7. Dong, S.-L., *et al.* (**2006**) A Photocontrolled β-Hairpin Peptide. *Chem. Eur. J. 12*, 1114-1120.

8. Schrader, T. E., *et al.* (**2007**) Light-triggered β-hairpin folding and unfolding. *P. Natl. Acad. Sci. USA 104*, 15729-15734.

9. Schrader, T. E., *et al.* (**2011**) Folding and Unfolding of Light-Triggered β-Hairpin Model Peptides. *J. Phys. Chem. B 115*, 5219-5226.

10. Hofmann, S. M., *et al.* (**2020**) Folding and Unfolding of the Short Light-Triggered β-Hairpin Peptide AzoChignolin Occurs within 100 ns. *J. Phys. Chem. B 124*, 5113-5121.

11. Deeg, A. A., *et al.* (**2011**) Light-Triggered Aggregation and Disassembly of Amyloid-Like Structures. *ChemPhysChem 12*, 559-562.

12. Chen, G. F., *et al.* (**2017**) Amyloid beta: structure, biology and structure-based therapeutic development. *Acta pharmacologica Sinica 38*, 1205-1235.

13. Hoppmann, C., *et al.* (**2012**) Light-Controlled Toxicity of Engineered Amyloid β-Peptides. *Chembiochem : a European journal of chemical biology 13*, 2657-2660.

14. Doran, T. M., *et al.* (**2012**) An Azobenzene Photoswitch Sheds Light on Turn Nucleation in Amyloid-β Self-Assembly. *ACS Chem. Neurosci. 3*, 211-220.

15. Nanda, J., *et al.* (**2017**) Emergence of native peptide sequences in prebiotic replication networks. *Nat. Commun. 8*, 434.

16. Rubinov, B., *et al.* (**2009**) Self-Replicating Amphiphilic β-Sheet Peptides. *Angew. Chem. Int. Edit. 48*, 6683-6686.

17. Bowerman, C. J., and Nilsson, B. L. (**2012**) Review self-assembly of amphipathic β-sheet peptides: Insights and applications. *Peptide Science 98*, 169-184.

18. Marini, D. M., *et al.* (**2002**) Left-Handed Helical Ribbon Intermediates in the Self-Assembly of a β-Sheet Peptide. *Nano Lett. 2*, 295-299.

19. Fitzpatrick, A. W. P., *et al.* (**2013**) Atomic structure and hierarchical assembly of a cross-β amyloid fibril. *P. Natl. Acad. Sci. USA 110*, 5468-5473.

20. Nelson, R., *et al.* (**2005**) Structure of the cross-beta spine of amyloid-like fibrils. *Nature 435*, 773-778.

21. Caplan, M. R., *et al.* (**2000**) Self-Assembly of a β-Sheet Protein Governed by Relief of Electrostatic Repulsion Relative to van der Waals Attraction. *Biomacromolecules 1*, 627-631.

22. Swanekamp, R. J., *et al.* (**2012**) Coassembly of Enantiomeric Amphipathic Peptides into Amyloid-Inspired Rippled β-Sheet Fibrils. *J. Am. Chem. Soc. 134*, 5556-5559.

23. Hwang, W.*, et al.* (**2003**) Supramolecular structure of helical ribbons self-assembled from a β-sheet peptide. *J. Chem. Phys. 118*, 389-397.

24. Clover, T. M.*, et al.* (**2020**) Self-Assembly of Block Heterochiral Peptides into Helical Tapes. *J. Am. Chem. Soc. 142*, 19809-19813.

25. Lee, N. R., Bowerman, C. J., and Nilsson, B. L. (**2013**) Effects of Varied Sequence Pattern on the Self-Assembly of Amphipathic Peptides. *Biomacromolecules 14*, 3267-3277.

26. Lee, N. R., Bowerman, C. J., and Nilsson, B. L. (**2013**) Sequence length determinants for self-assembly of amphipathic β-sheet peptides. *Peptide Science 100*, 738-750.

27. Betush, R. J., Urban, J. M., and Nilsson, B. L. (**2018**) Balancing hydrophobicity and sequence pattern to influence self-assembly of amphipathic peptides. *Peptide Science 110*, e23099.

28. Ivnitski, D.*, et al.* (**2014**) Introducing charge transfer functionality into prebiotically relevant β-sheet peptide fibrils. *Chem. Commun. 50*, 6733-6736.

29. Nakayama, K., Endo, M., and Majima, T. (**2005**) A Hydrophilic Azobenzene-Bearing Amino Acid for Photochemical Control of a Restriction Enzyme BamHI. *Bioconjugate Chem. 16*, 1360-1366.

30. Micsonai, A.*, et al.* (**2015**) Accurate secondary structure prediction and fold recognition for circular dichroism spectroscopy. *P. Natl. Acad. Sci. USA 112*, E3095-E3103.

31. Micsonai, A.*, et al.* (**2018**) BeStSel: a web server for accurate protein secondary structure prediction and fold recognition from the circular dichroism spectra. *Nucleic Acids Res. 46*, W315-W322.

32. Easterhoff, D.*, et al.* (**2011**) Enhancement of HIV-1 Infectivity by Simple, Self-Assembling Modular Peptides. *Biophys. J. 100*, 1325-1334.

33. Voropai, E. S.*, et al.* (**2003**) Spectral Properties of Thioflavin T and Its Complexes with Amyloid Fibrils. *J. App. Spec. 70*, 868-874.

34. Biancalana, M.*, et al.* (**2009**) Molecular Mechanism of Thioflavin-T Binding to the Surface of β-Rich Peptide Self-Assemblies. *J. Mol. Bio. 385*, 1052-1063.

35. Gade Malmos, K.*, et al.* (**2017**) ThT 101: a primer on the use of thioflavin T to investigate amyloid formation. *Amyloid 24*, 1-16.

36. Raz, Y.*, et al.* (**2013**) Effects of mutations in de novo designed synthetic amphiphilic β-sheet peptides on self-assembly of fibrils. *Chem. Commun. 49*, 6561-6563.

37. Hansen, A. L., and Kay, L. E. (**2014**) Measurement of histidine pKa values and tautomer populations in invisible protein states. *P. Natl. Acad. Sci. USA 111*, E1705-E1712.

38. Zhang, C.*, et al.* (**2017**) Switchable Hydrolase Based on Reversible Formation of Supramolecular Catalytic Site Using a Self-Assembling Peptide. *Angew. Chem. Int. Edit. 56*, 14511-14515.

39. Huang, Z.*, et al.* (**2013**) Self-assembly of amphiphilic peptides into bio-functionalized nanotubes: a novel hydrolase model. *J. Mat. Chem. B 1*, 2297-2304.

40. Guler, M. O., and Stupp, S. I. (**2007**) A Self-Assembled Nanofiber Catalyst for Ester Hydrolysis. *J. Am. Chem. Soc. 129*, 12082-12083.

41. Pettersen, E. F.*, et al.* (**2021**) UCSF ChimeraX: Structure visualization for researchers, educators, and developers. *Protein Sci. 30*, 70-82.

42. Pettersen, E. F.*, et al.* (**2004**) UCSF Chimera—A visualization system for exploratory research and analysis. *J. Comp. Chem. 25*, 1605-1612.

43. Hamley, I. W. (**2021**) Biocatalysts Based on Peptide and Peptide Conjugate Nanostructures. *Biomacromolecules 22*, 1835-1855.

44. Zozulia, O., Dolan, M. A., and Korendovych, I. V. (**2018**) Catalytic peptide assemblies. *Chem. Soc. Rev. 47*, 3621-3639.

45. Schindelin, J.*, et al.* (**2012**) Fiji: an open-source platform for biological-image analysis. *Nat. Methods 9*, 676-682.

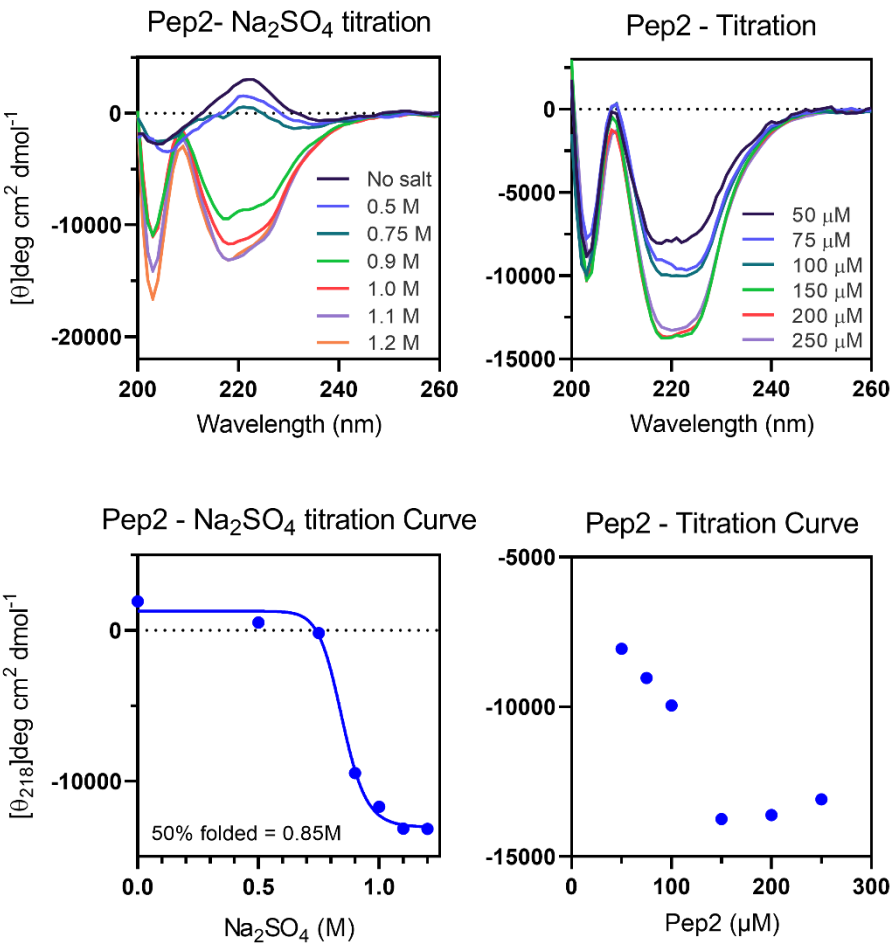

Figure S6.1: CD titrations of **Pep2**, showing the effect of salt (left) and peptide (right) concentration on self-assembly. Salt titrations were performed at a fixed peptide concentration of 100 µM, and peptide titrations with a fixed salt concentration of 1 M Na_2SO_4. Top figures show the entire CD spectra, with bottom figures showing the normalized absorption at 218 nm plotted against concentration. All samples contained 10 mM phosphate buffer at pH 7.4 and were measured at 20˚C.

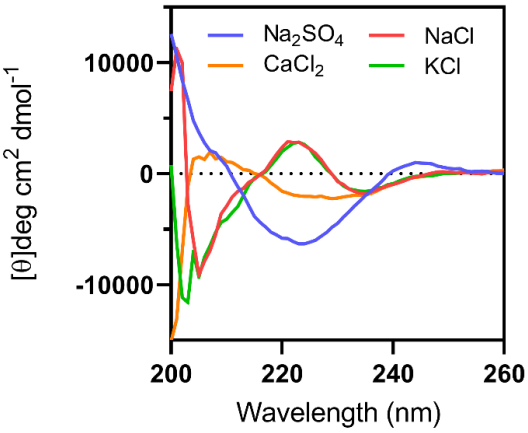

Figure S6.2: CD spectra of peptide **P6** in the presence of different salts. The peptide was thermally equilibrated and [peptide] = 100 µM. Salt concentration was 0.5 M, with 10 mM phosphate as buffer (pH 7.4) and were measured at 20˚C.

TEM image analysis

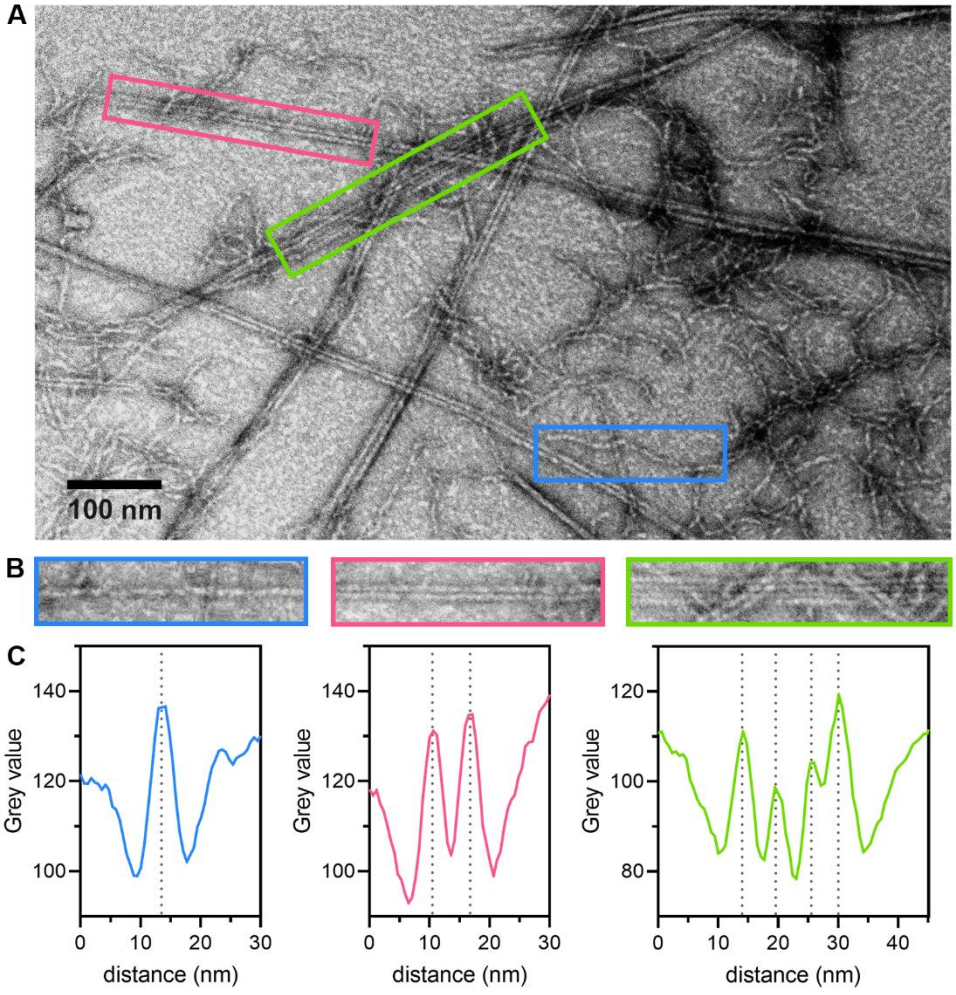

Figure S6.3: Representative TEM image showing the different types of structures observed for peptide **P2** (A). Structures are divided into 3 groups; single fibres (blue), double fibres (magenta) and structures comprised of multiple fibres (green). Straightened images (B) and derived profile plots (C) of selected fibres were prepared using Fiji. Dotted lines in the profile plots mark the center of peptide fibres.

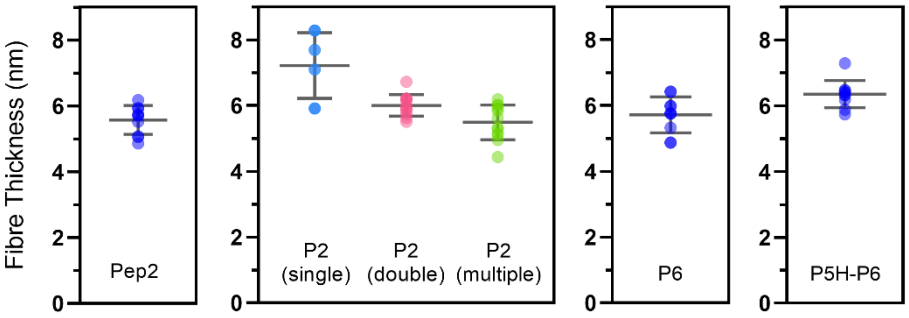

Figure S6.4: Size distribution of peptide fibres observed with TEM, with peptide **P2** divided in the three distinguishable groups of single, double, and multiple fibres as shown in **Figure S6.3**. Size distributions are also summarized in **Table S6.1**.

Table S6.1: Thickness and deviation of peptide fibres as observed via TEM (**Figure 6.2** and **Figure 6.7**) and Cryo-EM (**Figure 6.5**) and displayed graphically in **Figure S6.4**.

	Avg. Size (nm)	Std. Dev. (nm)	N fibres
Pep2	5.57	0.42	10
P2 (Single)	7.22	0.95	10
P2 (Double)	6.01	0.31	12
P2 (Multiple)	5.49	0.51	12
P6	5.71	0.52	10
P6 (Cryo-EM)	4.45	0.91	30
P5H-P6	6.35	0.39	10

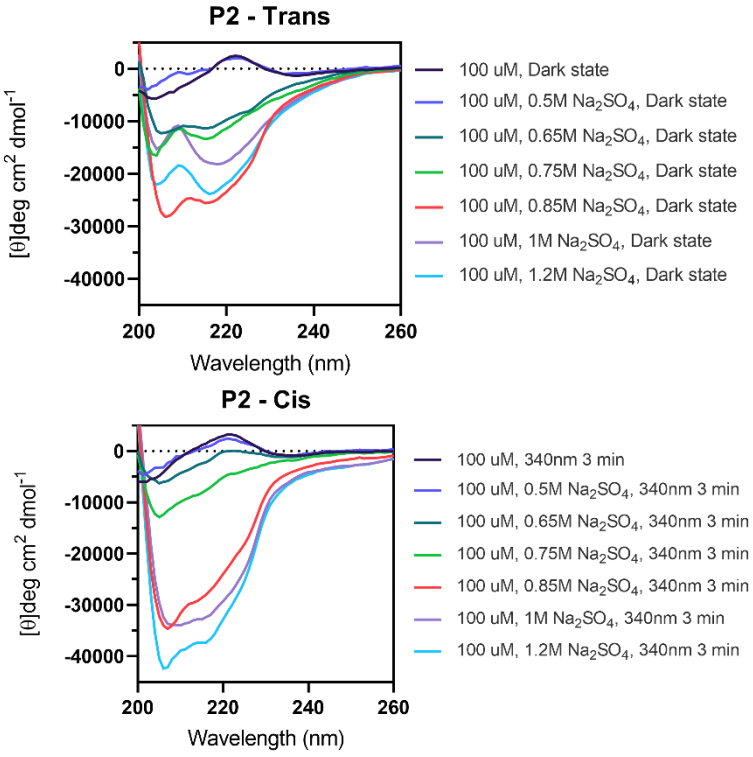

Figure S6.5: CD titration experiments to determine the effect of added salts on the structure of **P2** in the *trans* (dark, top) or *cis* (light, bottom) conformations. Measurements were performed at a 100 µM peptide concentration in 10 mM PB and were measured at 20 ˚C.

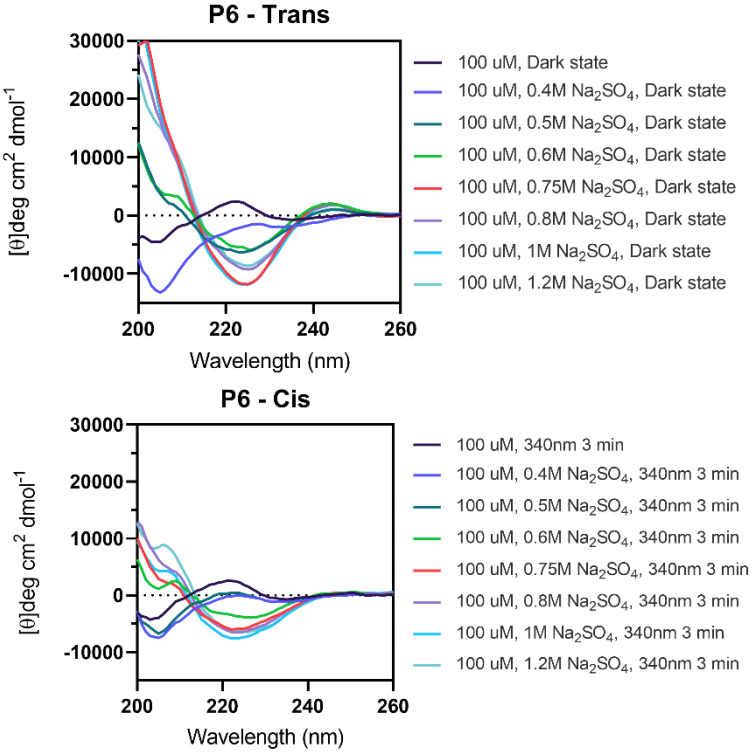

Figure S6.6: CD titration experiments to determine the effect of added salts on the structure of **P6** in the *trans* (dark, top) or *cis* (light, bottom) conformations. Measurements were performed at a 100 µM peptide concentration in 10 mM PB and were measured at 20 ˚C.

Table S6.2: Structural components (%) computed by the *BeStSel* web server from measured CD spectra in **Figure 6.2**. Legend: Anti1 = left-twisted β-strand; Anti2 = relaxed β-strand; Anti3 = right-twisted β-strand; Helix1 = regular α-helix; Helix2 = distorted α-helix; Para = Parallel β-strand. NRMSD = Normalised residual mean square deviation.

	Helix1	Helix2	Anti1	Anti2	Anti3	Para	Turn	Others	NRMSD
P6 340nm, 1M Na_2SO_4	0	0	14.96	4.14	6.06	0	18.33	56.51	0.049
P6 Dark, 1M Na_2SO_4	0	0	36.33	6.34	7.36	0	19.85	30.12	0.0182
P6 340nm	0	0	0	7.68	13.64	0	20.02	58.66	0.0794
P6 Dark	0	0	0	11.29	11.98	0	19.49	57.24	0.0754
P2 340nm, 1M Na_2SO_4	47.21	14.52	0	4.59	0	0	0.23	33.45	0.0467
P2 Dark, 1M Na_2SO_4	12.32	3.2	0	0	0	22.83	6.09	55.56	0.0585
P2 340nm	0	0	0	10.47	12.62	0	19.18	57.74	0.0719
P2 Dark	0	0	0	13.53	10.09	0	16.57	59.81	0.0733
Pep2, 1M Na_2SO_4	0	0	10.59	8.58	0	0.18	13.43	67.22	0.1262

Table S6.3: CAC values determined using DLS for peptides in thermal equilibrium (dark) and 340 nm irradiated state. Ratio indicates the fold increase in CAC for samples after irradiation.

	Dark (μM)	340nm (μM)	Ratio
P2, 1 M Na_2SO_4	6	29	4.8
P6, 0.6 M Na_2SO_4	22	109	5
P6, 1 M Na_2SO_4	11	20	1.8

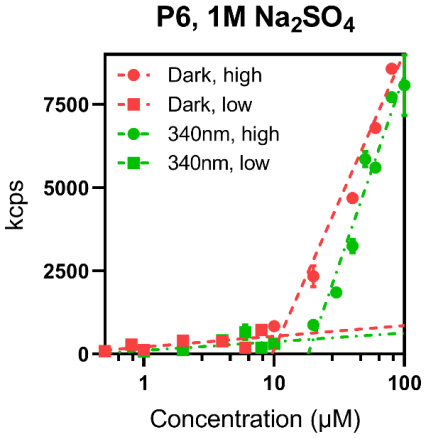

Figure S6.7: DLS determination of CAC of peptide **P6** with 1M Na_2SO_4, measured at 20 ˚C.

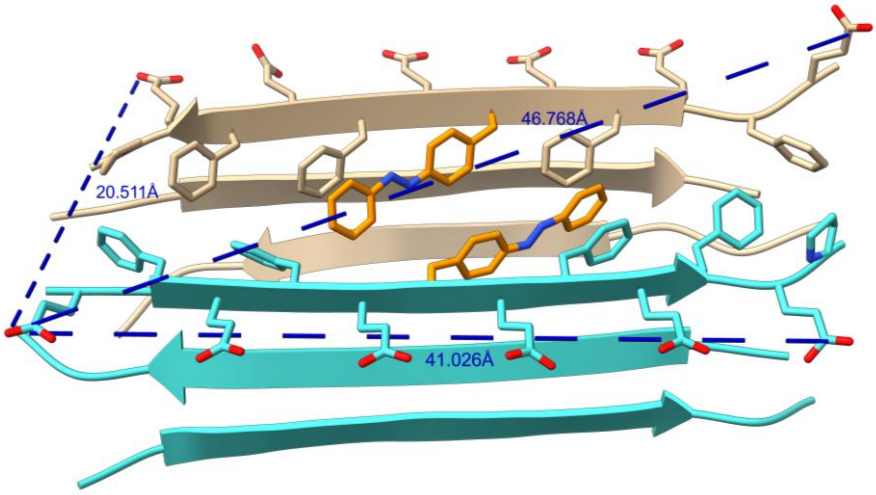

Figure S6.8: Image showing the calculated distances in a structural model of **P6** fibres assuming self-assembly into a double antiparallel β-sheet structure.

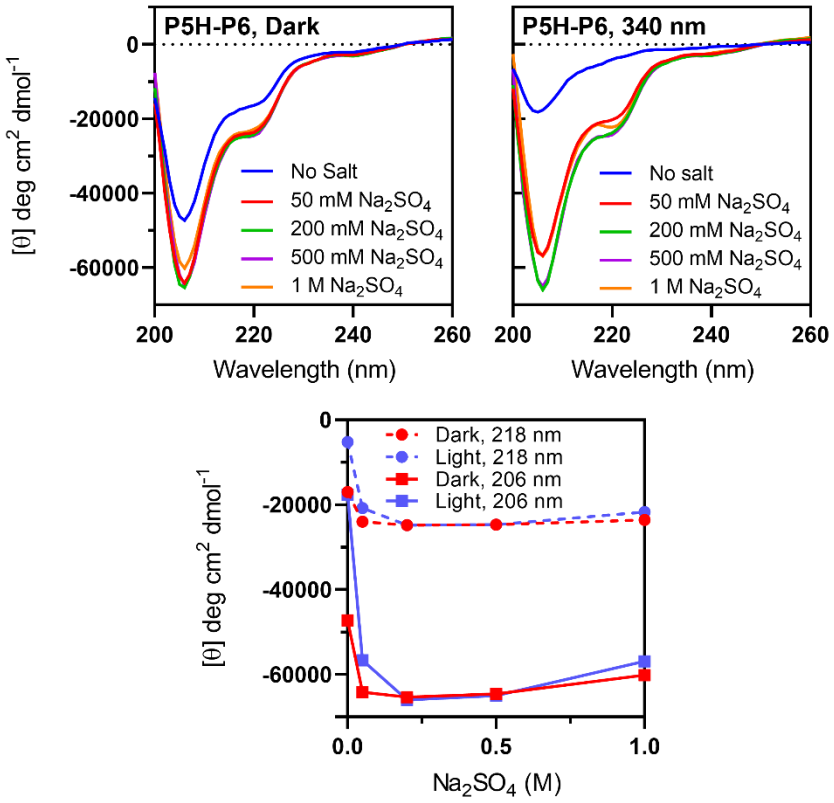

Figure S6.9: CD spectra of 100 µM **P5H-P6** in 10 mM phosphate buffer, with varying concentrations of Na_2SO_4 (top) and CD absorption at 218 or 206 nm versus the Na_2SO_4 concentration (bottom). Samples were measured at 20 ˚C and were either equilibrated in the dark or irradiated with 340 nm light to achieve PSS.

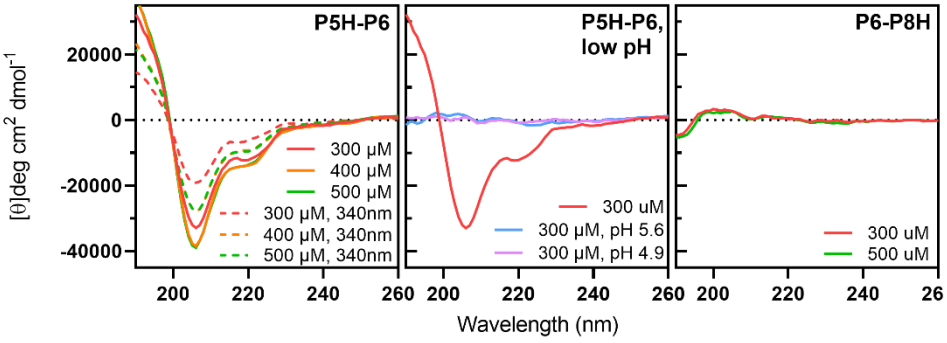

Figure S6.10: CD Spectra of peptides **P5H-P6** and **P6-P8H** at higher concentrations. Measured samples were equilibrated in the dark or irradiated with 340 nm light to achieve PSS. Samples contained 10 mM phosphate buffer and were measured at 20 ˚C.

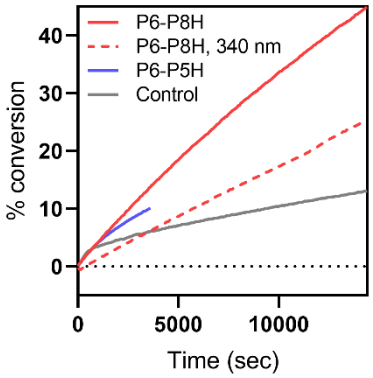

Figure S6.11: Kinetic hydrolysis curves of pNPA with different peptides as catalysts, performed at pH 6.0. The sample at 340 nm was illuminated before the start of the experiment, but not during the experiment.

Table S6.4: Overview of the catalytic parameters calculated from the kinetic hydrolysis experiments shown in **Figure 6.8** and **Figure S6.11**. Relative K_i is in comparison to the control samples of the same condition, with no peptide present. Turn over frequency (TOF) and K_i are calculated for the first 15 minutes of the experiment, unless noted otherwise.

Catalyst	Peptide (uM)	Dominant isomer	pH	K_i (s^{-1})	TOF (h^{-1})	Rel. K_i
No Peptide			7.5	1.80E-05		
P5H-P6	300	*Trans*	7.5	2.47E-05	0.016	1.38
P6-P8H	300	*Trans*	7.5	4.96E-05	0.076	2.76
P6-P8H	300	*Cis*	7.5	3.26E-05	0.035	1.81
P6-P8H	100	*Trans*	7.5	2.68E-05	0.068	1.49
No Peptide			6	2.72E-05		
P5H-P6	300	*Trans*	6	4.17E-05	0.035	1.54
P6-P8H	300	*Trans*	6	7.12E-05	0.105	2.62
No Peptide			6	1.76E-05[a]		
P6-P8H	300	*Trans*	6	3.11E-05[a]	0.053[a]	1.77
P6-P8H	300	*Cis*	6	2.59E-05[a]	0.021[a]	1.47

[a] *Values were calculated as the average over a 4-hour experiment.*

LC-MS of purified peptides

Table S6.5: Overview of the calculated masses of all peptides used in this project, and the masses observed by LCMS.

Peptide name	Calculated mass (Da)	Measured mass (Da)
Pep2	$[M - H^+]^-$ 1664.68	1665.10
P2	$[M - H^+]^-$ 1779.71	1769.51
P6	$[M - H^+]^-$ 1779.71	1686.85
P5H-P6	$[M + H^+]^+$ 1779.75	1778.50
P6-P8H	$[M + H^+]^+$ 1760.38	1761.72